27 May 2022

Enhancement of Cement Paste with Carboxylated Carbon Nanotubes and Poly(Vinyl Alcohol)

Yuyang Zhao

Jinrui Zhang

Gang Qiao

Dongshuai Hou

et. al. For a complete list of authors, see https://scholarsmine.mst.edu/civarc_enveng_facwork/2318

Recommended Citation

Y. Zhao et al., "Enhancement of Cement Paste with Carboxylated Carbon Nanotubes and Poly(Vinyl Alcohol)," *ACS Applied Nano Materials*, vol. 5, no. 5, pp. 6877 - 6889, American Chemical Society, May 2022.

The definitive version is available at https://doi.org/10.1021/acsanm.2c00875

ACS APPLIED NANO MATERIALS

www.acsanm.org Article

Enhancement of Cement Paste with Carboxylated Carbon Nanotubes and Poly(vinyl alcohol)

Yuyang Zhao, Jinrui Zhang,* Gang Qiao, Dongshuai Hou, Biqin Dong, and Hongyan Ma

Cite This: *ACS Appl. Nano Mater.* 2022, 5, 6877−6889 Read Online

ACCESS | Metrics & More | Article Recommendations | Supporting Information

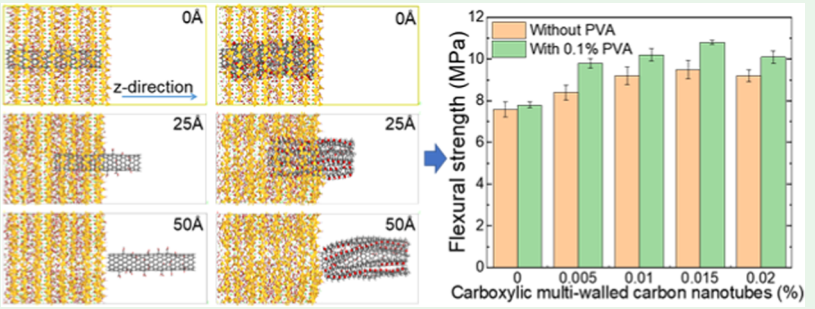

ABSTRACT: Cement has been a major consumable material for construction in the world since its invention, but its low flexural strength is the main defect affecting the service life of structures. To adapt cement-based materials to a more stringent environment, carboxylated carbon nanotubes (CNTs-COOH) and poly(vinyl alcohol) (PVA) are proposed to enhance the mechanical properties of cement paste. This study systematically verifies the synergistic effect of CNTs-COOH/PVA on the performance of cement paste. First, UV−Vis spectroscopy and FTIR spectroscopy prove that CNTs-COOH can provide attachment sites for PVA and PVA can improve the dispersion and stability of CNTs-COOH in water, which demonstrates the feasibility of synergistically enhancing cement paste. When a 0.015% CNTs-COOH suspension with 0.1% PVA is added, the flexural strength of the cement paste increases by 73, 32, and 42% compared with control specimens at curing ages of 3, 7, and 28 days, respectively. The strength enhancement mechanism is revealed from the aspects of cement matrix enhancement and interface enhancement. Thermogravimetric (TG) analysis and mercury intrusion porosimetry (MIP) prove that CNTs-COOH can enhance the hydration degree of the cement matrix and fill the pores introduced by PVA. Based on the fact that PVA can improve the dispersibility and the nucleation site effect of CNTs-COOH in cement paste, molecular dynamics simulation confirms that PVA can bridge CNTs-COOH and C−S−H to enhance the interfacial bonding by 64.1%.

KEYWORDS: *cement paste, carboxylated carbon nanotubes, poly(vinyl alcohol), enhancement, molecular dynamics*

1. INTRODUCTION

As the most widely used material in civil engineering, the low flexural resistance of cement-based materials is known as an important factor affecting the safety and durability of structures.[1,2] When the stress exceeds the flexural strength of cement-based materials under the action of temperature or load, it is easy to produce cracks.[3−6] In addition, the energy conservation and emission reduction policies of the cement industry have led to the limitation of cement production and consumption. To improve the flexural strength of cement-based materials and meet the strength requirements of concrete components with less cement, some researchers applied organic or inorganic materials to enhance cement-based materials.[7,8]

Since the invention of carbon nanotubes (CNTs) in 1991, CNTs have been extensively studied with their excellent mechanical and electrical properties.[9−12] CNTs also have been applied to cement-based materials to improve durability, increase mechanical strength, and avoid microcracks due to their small size and high strength.[13,14] However, Sobolkina et al. modified cement paste with CNTs, and the addition of CNTs had no positive effect on its static mechanical properties.[15] Lu et al. found that 0.05% CNTs could increase the flexural and compressive strength of cement paste by just 6.4 and 10.14%, respectively.[16] Isfahani et al. proved that the strength of a paste mortar containing CNTs was not significantly improved either by increasing the amount of CNTs or imposing sonication in mixing suspension.[17] The phenomenon that CNTs with excellent mechanical properties do not significantly improve the performance of a cement-based material is mainly attributed

Received: February 26, 2022
Accepted: April 12, 2022
Published: April 24, 2022

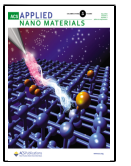

https://doi.org/10.1021/acsanm.2c00875
ACS Appl. Nano Mater. 2022, 5, 6877−6889

to two reasons: (1) the high van der Waals interaction energy results in poor dispersion of CNTs and (2) the inert CNTs cannot form strong interfacial bonding with cement-based materials.[18,19] To solve these problems, Li et al. used a mixture of a H_2SO_4 and HNO_3 solution for surface oxidation treatment (carboxylation) of CNTs to improve the hydrophilicity of CNTs.[20] The cement-based materials modified with CNTs-COOH can resist the erosion of harmful ions.[21] However, Savilov et al. showed that the cylindrical carbon nanotubes are mainly formed by sp^2-hybrid carbon atoms, and the interface problem cannot be solved solely by the few carboxyl groups produced at the defects.[22] Meanwhile, the cationic bridging effect is formed between functionalized CNTs through Ca^{2+}, presenting significant agglomeration in cement-based materials.[23] Therefore, well dispersion of CNTs in a cement matrix may not be obtained by functionalizing CNTs, and its application in cement-based materials requires the assistance of a more efficient dispersion method.

PVA is an extremely safe organic compound that is considered to be the only soluble biodegradable polymer and is widely employed in composites due to its excellent chemical and mechanical stability.[24−27] The compressive strength of the cement mortar increased by 12.15% for a PVA content of 0.6% and the flexural strength of the cement mortar increased by 24.83% for a PVA content of 1.0% in the study of Fan et al.[28] On the contrary, Pique et al. found that 4% PVA reduced the compressive strength of cement paste by about 20% while slightly increasing the flexural strength, which was the same as the research result of Lu et al.[29,30] This was attributed to the increased porosity of the cement paste after adding PVA, as PVA could reduce mechanical properties of cement-based materials by introducing bubbles that were difficult to remove.[31]

In this study, CNTs-COOH and PVA are used to enhance the cement paste, according to the application precedents of PVA and CNTs.[32−34] The hydroxyl group of PVA can form hydrogen bonding or ionic bonding with the carboxyl group of CNTs-COOH and C−S−H of cement-based materials.[35−37] In addition, well-dispersed CNTs-COOH can optimize the pore structure of cement-based materials.[38,39] Based on the above two points, this paper hypothesizes that PVA could improve the dispersion and enhance the interface of CNTs-COOH, while CNTs-COOH could fill the pores introduced by PVA, thereby synergistically enhancing the performance of cement paste. This hypothesis is systematically studied from multiple perspectives. The suspension properties are preliminarily explored by UV−Vis spectrophotometry (UV−Vis) and Fourier transform infrared (FTIR) spectroscopy. The macroscopic mechanical enhancement of cement paste is quantified by a mechanical test. The effect of CNTs-COOH and PVA on the hydration process and pore structure of the cement matrix are analyzed by X-ray diffraction (XRD), thermogravimetric (TG) analysis, and mercury intrusion porosimetry (MIP). Meanwhile, environmental scanning electron microscopy (ESEM), energy dispersive spectrometry (EDS), and molecular dynamics simulation are applied to characterize the interface between CNTs-COOH and the cement matrix at the micro- and molecular scale.

2. METHODOLOGY

2.1. Materials. In this experiment, ordinary Portland cement conforming to the requirements of ASTM C150 Type I was used, chemical compositions of which are shown in Table S1. PVA powder (160-mesh) was selected for the experiment. An isothermal heating magnetic stirring device was employed to dissolve the PVA powder and the temperature was maintained at 75 °C until the powder was fully dissolved. The CNTs used in the experiment are CNTs-COOH, which is a kind of oxidized CNTs. The physical properties and morphology are shown in Table S2 and Figure S1.

2.2. Experimental Methods of CNTs-COOH/PVA Suspensions. *2.2.1. Preparation of Suspensions.* The preparation method of CNTs-COOH/PVA suspensions is the basis of cement paste preparation. First, CNTs-COOH and water were added to a beaker in a mass ratio of 0.1:100, and the premix was obtained after mechanical stirring for 5 min and ultrasonic dispersion for 15 min. Then, the CNTs-COOH premix, PVA solution, and water were mixed according to the proportion, and the suspensions used in the experiment were obtained after continued ultrasonic dispersion for 15 min. In the suspensions, the concentration of PVA was controlled at 0 or 0.1%, and the ratio of CNTs-COOH to water was fixed at 0−0.02% with an increase of 0.005%. The concentration of PVA and CNTs-COOH was calculated according to eqs 1 and 2. The mixing ratios of the suspensions are listed in Table S3.

$$C_p = \frac{m_p}{m_p + m_c + m_w} \times 100\% \quad (1)$$

$$C_c = \frac{m_c}{m_p + m_c + m_w} \times 100\% \quad (2)$$

where C_p and C_c are concentrations of PVA and CNTs-COOH, respectively, and m_p, m_c, and m_w are the masses of PVA, CNTs-COOH, and water (g), respectively.

2.2.2. UV−Vis Test. The suspensions were placed in a transparent glass bottle and allowed to stand for 72 h to observe their dispersion state. Meanwhile, a TU-1901 UV−Vis spectrometer was employed to measure the absorbance of the suspensions with a wavelength of 260 nm.[40]

2.2.3. FTIR Test. FTIR was applied to analyze the connections between PVA and CNTs-COOH. The ratio of CNTs-COOH to PVA in a suspension was 1:10, and the measured sample was the sediment of the suspension after centrifugation. An FTIR test was performed using a Bucks HP9 2FX infrared spectrometer produced by PerkinElmer in the United States.

2.3. Experimental Methods of CNTs-COOH/PVA Cement Paste. *2.3.1. Preparation of Cement Paste.* To study the enhancement effect of CNTs-COOH/PVA on cement, cement paste without an aggregate was employed for experiments. The water−cement ratio of cement paste specimens was fixed at 0.38. The suspensions in Section 2.2.1 were used for mixing with cement, that is, the ratio of PVA to water was fixed at 0 or 0.1% and the ratio of CNTs-COOH to water was fixed at 0−0.02% with an increase of 0.005%. First, the suspension was added to the cement. After mixing and stirring for 2 min, the paste was poured into molds with a size of 40 mm × 40 mm × 160 mm and 50 mm × 50 mm × 50 mm. After curing for 24 h, the mold was removed. When cement paste had the required curing age, the macroscopic mechanical strength test and microscopic characterization were employed.

2.3.2. XRD and TG/DTA Tests. XRD was applied to analyze the influence of CNTs-COOH and PVA on hydration progress and products. A SmartLab X-ray diffractometer produced by Rigaku in the United States was adopted for the XRD test.

TG and differential thermal analysis (DTA) were used to conduct thermal analysis of cement paste. The test specimens were the same as XRD. The test instrument was an HCT-3

https://doi.org/10.1021/acsanm.2c00875
ACS Appl. Nano Mater. 2022, 5, 6877−6889

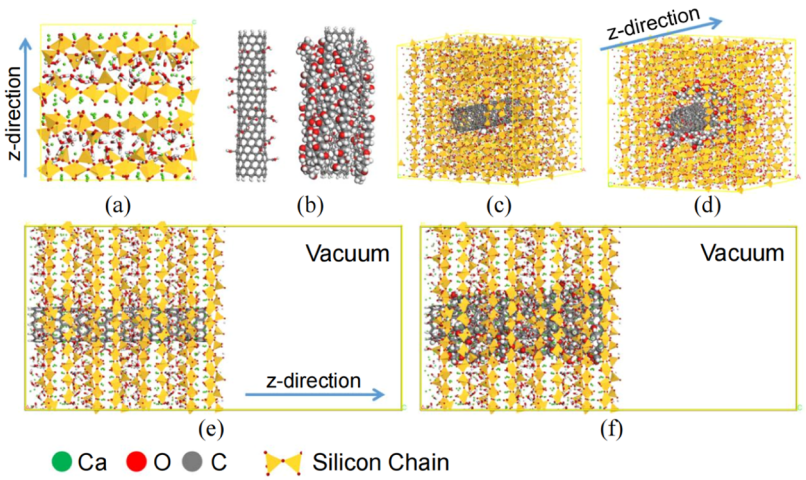

Figure 1. Molecular models of (a) C−S−H cell, (b) CNTs-COOH and CNTs-COOH/PVA, (c) CNTs-COOH/C−S−H, (d) CNTs-COOH/PVA/C−S−H, (e) CNTs-COOH/C−S−H with the vacuum, and (f) CNTs-COOH/PVA/C−S−H with the vacuum.

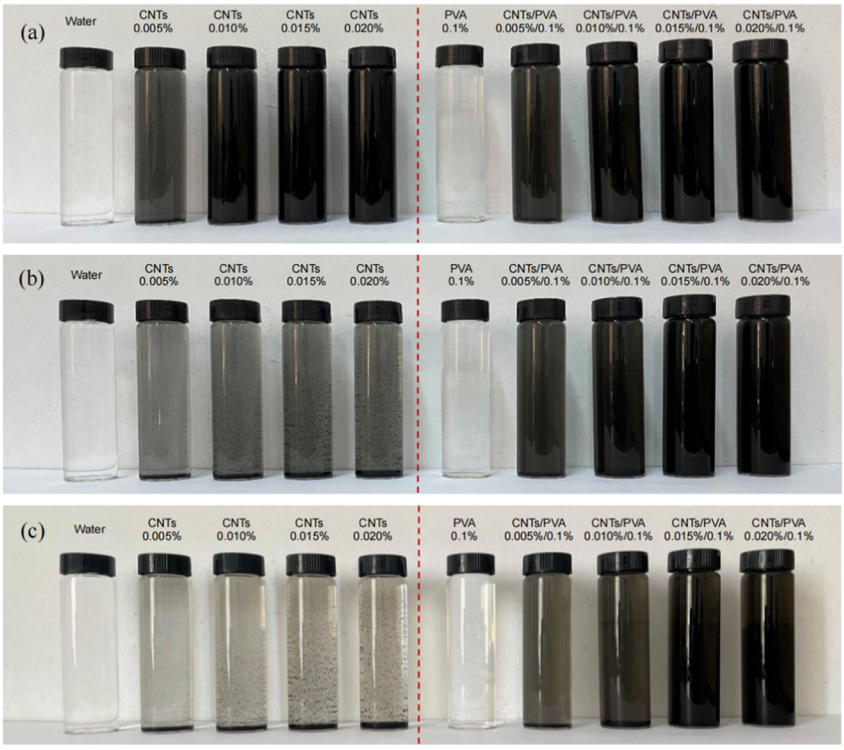

Figure 2. Static images of water, CNTs-COOH suspensions, PVA solution, and CNTs-COOH/PVA suspensions at (a) 0 h, (b) 2 h, and (c) 72 h.

comprehensive thermal analyzer produced by Hengjiu in Beijing. The test temperature range was 30−940 °C and the heating rate was 10 °C/min.

2.3.3. MIP Test. MIP test was used to analyze the pore distribution of the hardened cement paste. The MIP test adopts a Micromeritics Autopore IV 9510 automatic mercury intrusion porosimeter, according to tips recommended in papers.[41,42]

2.3.4. ESEM and EDS Tests. ESEM was used to observe the dispersion of CNTs-COOH in the cement paste with or without PVA. EDS was employed to observe the nucleation site effect for hydration products on the CNTs-COOH surface in cement paste. The nucleation site effect is that well-dispersed CNTs-COOH can adsorb surrounding hydration products.[43] A Quanta FEG 250 field emission environmental scanning electron microscope produced by ZISS in Germany was applied for ESEM and EDS tests.

2.3.5. Molecular Dynamics Simulation. To verify the interface enhancement of PVA between CNTs-COOH and cement-based materials at a molecular level, molecular dynamics simulation was used in this study. First, the C−S−H gel molecular model was used as established in the previous study.[44] The C−S−H model was modified from tobermorite, which had a similar laminar structure to C−S−H. The calcium to silicon ratio of model was 1.3 and the lattice parameters were a = 22.05 Å, b = 21.90 Å, c = 22.49 Å, and $\alpha = \beta = \gamma = 90°$, as shown in Figure 1a. CNTs-COOH with a diameter of 7.7 Å and a length of 43 Å was employed and 5 wt % carboxyl groups were randomly modified on its surface, as shown in Figure 1b. Subsequently, PVA was wrapped on the surface of functionalized carbon

https://doi.org/10.1021/acsanm.2c00875
ACS Appl. Nano Mater. 2022, 5, 6877−6889

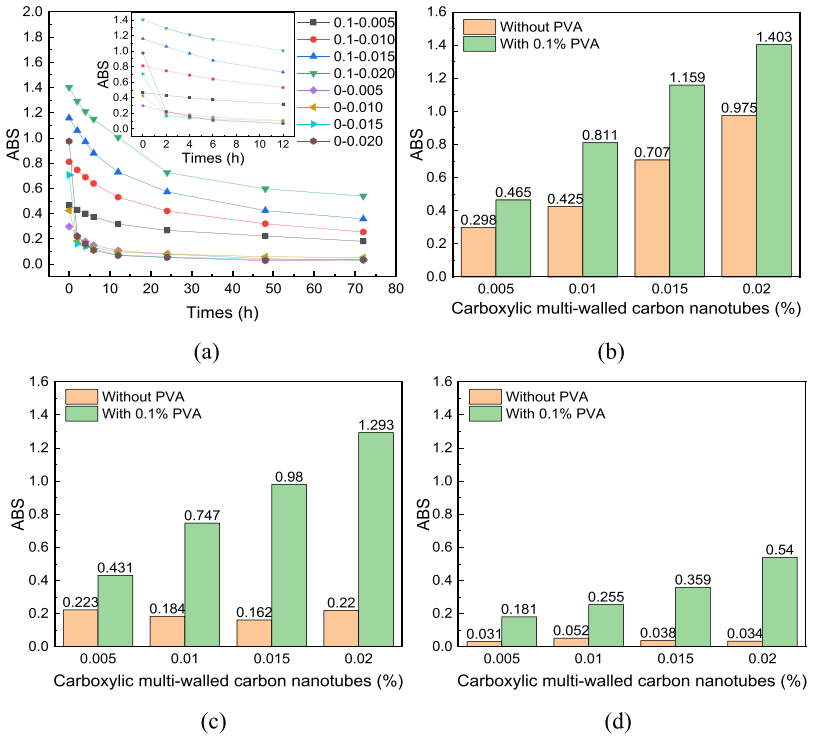

Figure 3. UV−Vis ABS of suspensions at a wavelength of 260 nm (a) during 72 h, (b) at 0 h, (c) at 2 h, and (d) at 72 h.

nanotubes (Figure 1b). The established C−S−H model constituted of a 2 × 2 × 2 unit cell was dug in the direction perpendicular to the calcium−silica layers throughout the cell to be able to accommodate CNTs-COOH and PVA. The established CNTs-COOH/C−S−H and CNTs-COOH/PVA/C−S−H composites are shown in Figure 1c,d. To enable the pull-out simulation, after the above model reaches equilibrium (introduced in Section 3.2.5), the periodic boundary in the *z*-direction of the model was broken. After this, a vacuum was reserved in the *z*-direction (Figure 1e,f), so the reinforcing material could be pulled out.

The whole simulation was divided into two stages: the pre-equilibration stage and the pull-out stage. All simulations were run on the LAMMPS platform. In the prebalancing stage, the system was relaxed and the NPT ensemble was applied. Meanwhile, the time step, pressure, and temperature were set to 1 fs, 1 kPa, and 300 K. The whole prebalancing stage lasted 5 ns and the traces were output and saved every 1 ps, obtaining 5000 frames for microstructure analysis at the interface. The periodic boundary in the *z*-direction of the already equilibrated configuration was broken and a vacuum was left. In the pull-out simulation stage, the ensemble was changed to NVT and the temperature or time step was kept constant. The CNTs-COOH and PVA were pulled out together from the C−S−H matrix by applying a spring force on the selected atoms of CNTs-COOH and PVA. The spring force was set as following eq 3

$$F = K((x_1 + v \times t) - x_{com}) \quad (3)$$

where F stands for the spring force; K represents the spring constant (0.01 kcal/mol·nm^2); and x_1, v, t, and x_{com} stand for the initial mass center position of the selected atoms, pulling speed (0.0025 nm/ps), simulation time, and the real-time location of the mass center position of the selected atoms. The whole pull-out stage lasted 2 ns and the pull-out load−displacement curve was obtained during the whole simulation process.

CSHFF was used to describe the C−S−H matrix, which was proved to be good at describing the structure of C−S−H as well as mechanical properties such as elastic properties.[45−47] CVFF was used to simulate functionalized carbon nanotubes as well as PVA, which has been proved to be excellent in simulating the conformational and thermodynamic properties of organic materials.[3,48] The interaction of the two force fields was generated by Lorentz−Berthelot mixing rules. The fusion of CSHFF and CVFF could effectively simulate the mechanical properties of organic−inorganic composites and the enhancement at the interface.[49−51]

3. RESULTS AND DISCUSSION

3.1. Analysis of CNTs-COOH/PVA Suspensions. Studying the dispersibility of CNTs-COOH in water and its interaction with PVA is the basis for the application of CNTs-COOH and PVA in cement paste, which is helpful for the analysis and understanding of the subsequent research on cement paste.

3.1.1. Dispersion Enhancement of CNTs-COOH in Water. Figure 2 shows the standing state of CNTs-COOH suspensions with or without PVA. Figure 2a shows the suspensions after 30 min of ultrasonic dispersion, but the effect of adding PVA on the dispersion of CNTs-COOH cannot be observed. CNTs-COOH suspensions without PVA show a large amount of agglomeration and precipitation after standing for 2 h, while CNTs-COOH suspensions with 0.1% PVA maintain a high concentration after 72 h, as shown in Figure 2b,c. This phenomenon confirms that PVA keeps CNTs-COOH dispersed for a longer period of time in water.

The effect of PVA on the dispersion of CNTs-COOH in water was quantitatively analyzed by UV−Vis. Figure 3a shows the change in UV−Vis absorbance (ABS) of CNTs-COOH with different concentrations during 72 h. To visually observe the difference between the suspensions before and after adding

https://doi.org/10.1021/acsanm.2c00875
ACS Appl. Nano Mater. 2022, 5, 6877−6889

PVA, the ABS values of suspensions at 0, 2, and 72 h are shown in Figure 3. The ABS of all suspensions at 0 h increased with the CNTs-COOH content. When the concentrations of CNTs-COOH are 0.005, 0.01, 0.015, and 0.02%, the ABS of the suspensions is 0.298, 0.425, 0.707, and 0.975, respectively. After the addition of 0.1% PVA, the ABS of the suspensions increases by 56, 91, 64, and 44%, respectively, indicating that PVA can improve the dispersibility of CNTs-COOH in an aqueous solution. In addition, the ABS of CNTs-COOH suspensions without PVA decreases rapidly within 2 h of standing, while that of CNTs-COOH/PVA suspensions declines slowly during the 72 h test. Therefore, PVA can improve the dispersion and stability of CNTs-COOH in water, laying the foundation for the dispersion of CNTs-COOH in cement paste, which is the same as the results in the standing experiment.

3.1.2. PVA Attachment on CNTs-COOH. In this section, the ratio of CNTs-COOH to PVA in suspension is 1:10, and the measured samples are PVA power, CNTs-COOH, and sediment of the CNTs-COOH/PVA suspension after centrifugation. According to the FTIR of CNTs-COOH shown in Figure 4, the

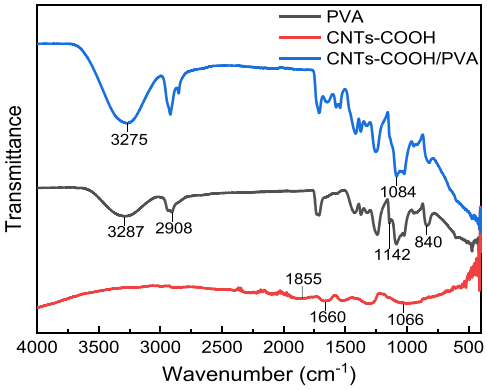

Figure 4. FTIR spectra of PVA, CNTs-COOH, and CNTs-COOH/PVA.

characteristic peaks at 1066, 1855, and 1660 cm^{-1} represent the C−O, C═O, and C═C bond stretching vibrations of CNTs-COOH.[36,52] In the infrared spectra of PVA, the characteristic peaks at 840, 1142, 2908, and 3287 cm^{-1} represent the stretching vibrations of C−C, C−O, C−H, and O−H bonds.[53,54] By FTIR spectroscopy of precipitate in the CNTs-COOH/PVA suspension, it can be seen that a large number of bonds' stretching vibrations belong to PVA. Since PVA can be stably dissolved in water, the PVA in the sediment is due to its attachment on the surface of CNTs-COOH. Meanwhile, the characteristic peak of C−O shifts from 1142 to 1084 cm^{-1} due to the hydrogen bonding between the −OH groups of PVA and the −COOH groups of the CNTs-COOH.[35] The attachment of PVA on CNTs-COOH surface explains why PVA can improve the dispersion and stability of CNTs-COOH in water.

The standing test, UV−Vis spectra, and FTIR spectra demonstrate that the adsorption of PVA on the surface of CNTs-COOH improves the dispersion of CNTs-COOH in water, which provides the feasibility for the subsequent application of CNTs-COOH/PVA suspensions in cement paste. The effect of CNTs-COOH and PVA on the properties of cement paste and the effect mechanism are described below.

3.2. Analysis of CNTs-COOH/PVA Cement Paste. *3.2.1. Mechanical Enhancement of Cement Paste.* When the suspensions are added to the cement according to the water−cement ratio, the mechanical strength of the cement paste is improved to different degrees. Figure 5a−c shows the flexural strength of cement paste mixed with CNTs-COOH and PVA. The flexural strength of CNTs-COOH cement paste without PVA first increases and then decreases with increasing CNTs-COOH content. This is the same trend as the research by Cui et al., although the CNTs-COOH content is different.[55] The maximum strength of cement paste is obtained when the content of CNTs-COOH in the suspension is 0.015%, which increases by 50, 11, and 25% at 3, 7, and 28 days, respectively. The variation trend of flexural strength of CNTs-COOH cement paste with PVA was the same as that without PVA and the flexural strength of cement paste mixed with a 0.015% CNTs-COOH/0.1% PVA suspension is 73, 32, and 42% higher than the control specimen at 3, 7, and 28 days, respectively. The strength declines with the increase of CNTs-COOH due to the entanglement of CNTs-COOH. PVA may improve the dispersion or nucleation of CNTs but does not change the inflection point of its enhancement.

The variation trend of the compressive strength is similar to that of flexural strength but the reinforcement is weaker, as shown in Figure 5d−f. Furthermore, a 0.1% PVA solution has no effect on the strength of cement paste. Therefore, the main reason for the mechanical enhancement of cement paste is the synergistic effect of PVA and CNTs-COOH. In addition, the significant increase in the flexural strength in 3 days is related to the hydration process of cement, and the reason why the flexural strength is much higher than the compressive strength is that the flexural strength is more sensitive to the pore structure. Enhancement mechanism studies will explain these accordingly.

3.2.2. Hydration Degree Enhancement of Cement Paste. The hydration degree and hydration products are closely related to the mechanical strength of cement-based materials. XRD and TG/DTA are used to qualitatively and quantitatively analyze the hydration degree of cement paste. In this section, the CNTs-COOH and PVA concentrations of the suspensions used for cement paste mixing are 0.015 and 0.1%, respectively. The analysis results are as follows:

According to the XRD spectrum analysis, the peak values of $Ca(OH)_2$ in cement paste specimens with PVA and CNTs-COOH/PVA are significantly higher than the control specimen and the CNTs-COOH specimen at 3 and 7 days, indicating that PVA can improve the hydration rate of cement at the early hydration stage, as shown in Figure 6a,b. In addition, high content of $Ca(OH)_2$ can improve the early strength of cement paste and also provide a better formation environment for C−S−H to improve the later strength. In Figure 6c, at the age of 28 days, the $Ca(OH)_2$ content of the specimen with PVA is higher than other specimens, while the $Ca(OH)_2$ peak value of the CNTs-COOH/PVA specimen decreased. To explain this phenomenon and quantitatively analyze the hydration degree of cement paste, TG/DTA was carried out.

According to the descending trend of TG curves and the endothermic valleys of DTA curves shown in Figure 7, it can be seen that the main hydration products of cement paste are C−S−H, AFt, $Ca(OH)_2$, and $CaCO_3$, which are the same as the results of XRD. The TG mass loss of the specimens with a PVA solution and a CNTs-COOH/PVA suspension is the maximum at 3, 7, and 28 days, indicating the breakdown of more hydration products.

In general, the decomposition of cement hydrate can be divided into three temperature ranges, which represent the dehydration of C−S−H, the dehydroxylation of $Ca(OH)_2$, and

https://doi.org/10.1021/acsanm.2c00875
ACS Appl. Nano Mater. 2022, 5, 6877−6889

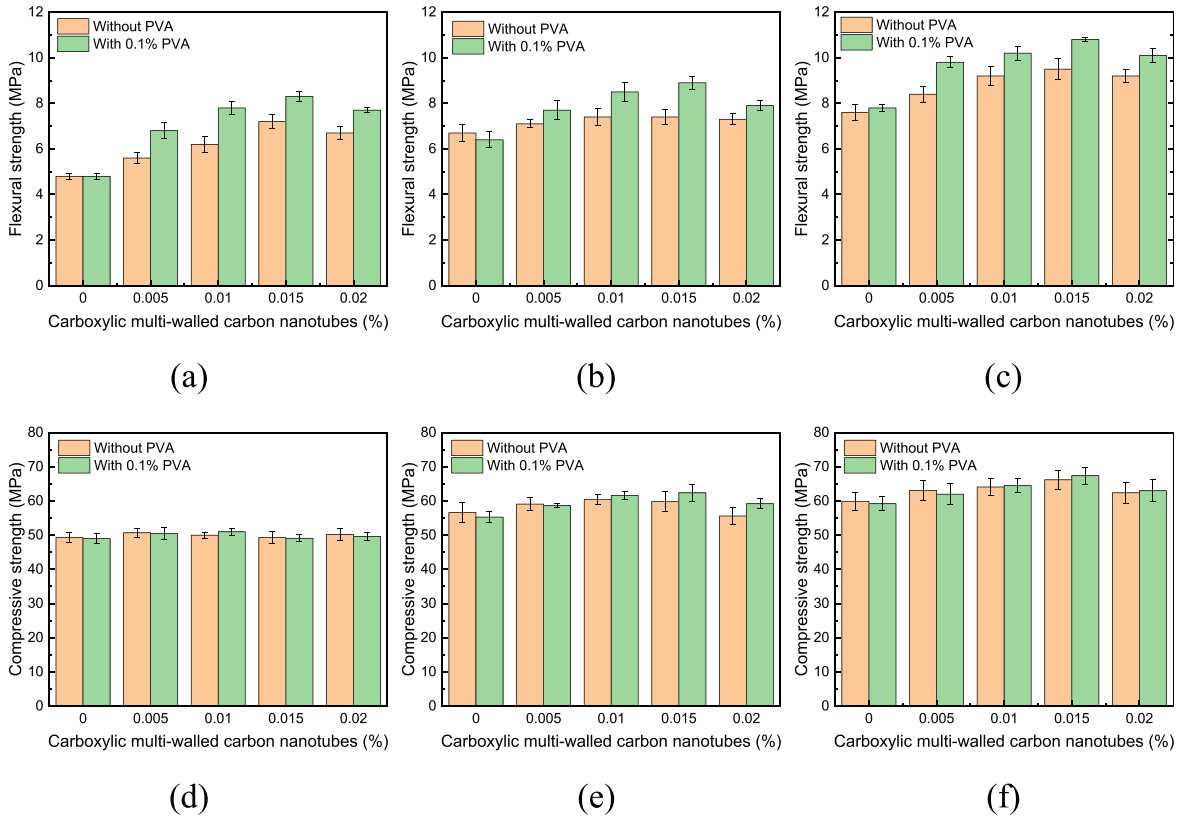

Figure 5. Flexural strength and compressive strength of cement paste with water, PVA solution, CNTs-COOH suspensions, and CNTs-COOH/PVA suspensions at (a, d) 3 days, (b, e) 7 days, and (c, f) 28 days.

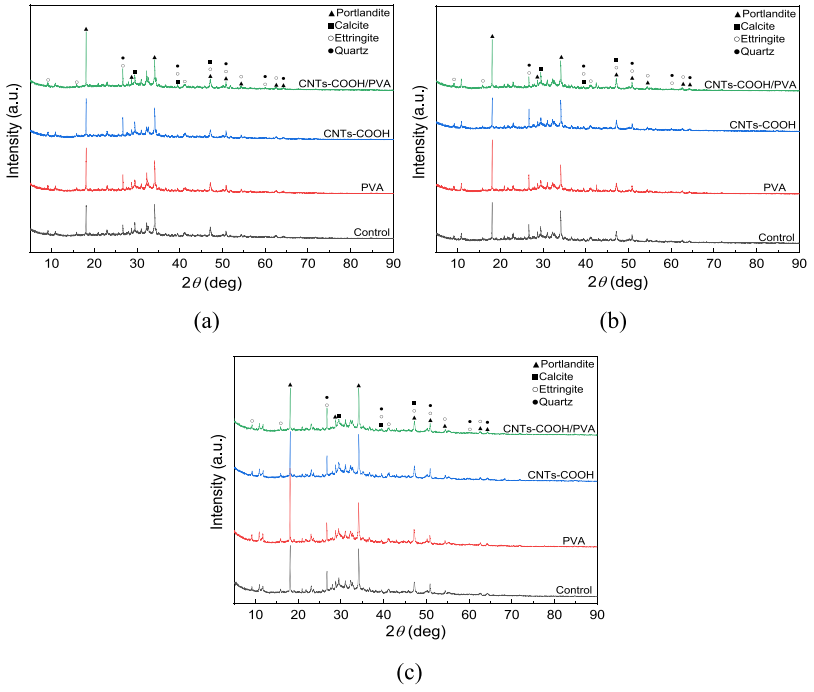

Figure 6. XRD spectra of the cement paste mixed with water, PVA solution, CNTs-COOH suspension, and CNTs-COOH/PVA suspension at (a) 3 days, (b) 7 days, and (c) 28 days.

the decarbonation of $CaCO_3$.[56] To quantitatively analyze the hydration degree of cement paste and the content of $Ca(OH)_2$, eqs 4−6 are proposed in this paper, combined with the calculation methods of Monteagudo, Pane, Mounanga, and Ahmed.[57−60] The content of $CaCO_3$ should be taken into account when calculating the content of $Ca(OH)_2$.

$$W_B = L_{dh1} + L_{dh2} + (L_{dh3} - L_{dc}) + \frac{18}{44}L_{dc} \quad (4)$$

https://doi.org/10.1021/acsanm.2c00875
ACS Appl. Nano Mater. 2022, 5, 6877−6889

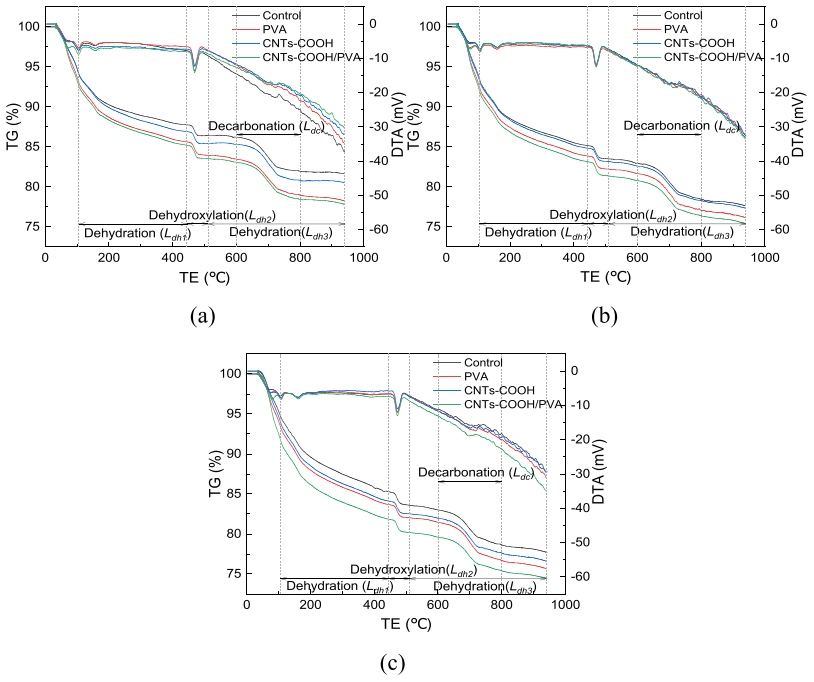

Figure 7. TG/DTA curves of the cement paste with water, PVA solution, CNTs-COOH suspension, and CNTs-COOH/PVA suspension at (a) 3 days, (b) 7 days, and (c) 28 days.

$$\alpha = \frac{W_B}{W_{B\infty}} \tag{5}$$

$$W_{CH} = \frac{74}{18}\left(L_{dh2} + \frac{18}{44}L_{dc}\right) \tag{6}$$

where W_B is the total mass loss of chemically bound water in the TG curve; L_{dh1}, L_{dh2}, L_{dh3}, and L_{dc}, respectively, represent the mass loss corresponding to the dehydration of C−S−H, dehydroxylation of $Ca(OH)_2$, decomposition of other hydration products, and decarburization of $CaCO_3$; $\frac{18}{44}$ is the molar mass ratio of H_2O to CO_2; α is the hydration degree of cement paste; $W_{B\infty}$ represents the chemical bound water content of cement paste after complete hydration, take $W_{B\infty}$ = 0.23; W_{CH} is $Ca(OH)_2$ content; and $\frac{74}{18}$ is the molar mass ratio of $Ca(OH)_2$ to H_2O.

Combined with the decomposition temperature limits between C−S−H, $Ca(OH)_2$, and $CaCO_3$ of various researchers, the temperature ranges and corresponding mass losses of L_{dh1}, L_{dh2}, L_{dh3}, and L_{dc} are assigned, as shown in Figure 7 and Table 1.[56−61] The hydration degree coefficient α and $Ca(OH)_2$ content W_{CH} of each cement paste specimen at different ages calculated according to eqs 4−6 are shown in Table 1.

As shown in Table 1, the hydration degree of the CNTs-COOH/PVA cement paste specimen is higher than other specimens during the curing process. The hydration degrees are 52.95, 60.35, and 66.60% at 3, 7, and 28 days, respectively. This is an important factor for the strength enhancement of the cement paste mixed with the CNTs-COOH/PVA suspension. In particular, the CNTs-COOH/PVA suspension and the CNTs-COOH suspension significantly improve the 3 days' hydration degree of cement paste, which are 9.4 and 5.14% higher than that of the control specimen, explaining the significant flexure enhancement of cement paste at 3 days. Meanwhile, the addition of CNTs-COOH/PVA increases the $Ca(OH)_2$ content of the cement paste at 3 days but decreases at 28 days. Under the condition of the higher hydration degree α at 28 days, the low content of $Ca(OH)_2$ represents the increase of other hydration products. Han et al. found that nanofillers with nonpozzolanic activity could accelerate the formation of C−S−H by increasing the $Ca(OH)_2$ content at an early age, preventing the large size of $Ca(OH)_2$ crystals, and changing the orientation index of $Ca(OH)_2$ crystals to reduce the structural defect.[62] The above phenomena are consistent with the variation trend of $Ca(OH)_2$ in specimens with CNTs-COOH. In addition, the content of $Ca(OH)_2$ in the cement paste mixed with a PVA solution reaches 14.75% at 3 days, which provides a good environment for the formation of C−S−H. In summary, the

Table 1. Mass Loss at Different Temperature Ranges, Degree of Hydration, and $Ca(OH)_2$ Content (%)

	temperature range (°C)	age (days)	control	PVA	CNTs-COOH	CNTs-COOH/PVA
L_{dh1}	105−440	3	6.41	7.44	7.22	7.39
		7	8.23	8.49	8.32	8.74
		28	9.46	9.95	9.94	9.77
L_{dh2}	440−520	3	1.36	1.74	1.48	1.75
		7	1.71	1.71	1.74	1.86
		28	1.80	1.73	1.67	1.76
L_{dh3}	520−940	3	4.76	5.65	4.91	5.67
		7	5.84	6.03	5.79	5.87
		28	5.84	5.65	5.92	6.28
L_{dc}	600−800	3	4.26	4.5	4.48	4.64
		7	4.45	4.61	4.31	4.39
		28	4.37	4.75	4.35	4.22
degree of hydration α		3	43.55	52.47	47.69	52.95
		7	57.18	58.75	57.88	60.35
		28	63.16	63.17	65.08	66.60
$Ca(OH)_2$ content		3	12.77	14.75	13.64	15.00
		7	14.53	14.81	14.42	15.04
		28	14.77	15.13	14.22	14.33

https://doi.org/10.1021/acsanm.2c00875
ACS Appl. Nano Mater. 2022, 5, 6877−6889

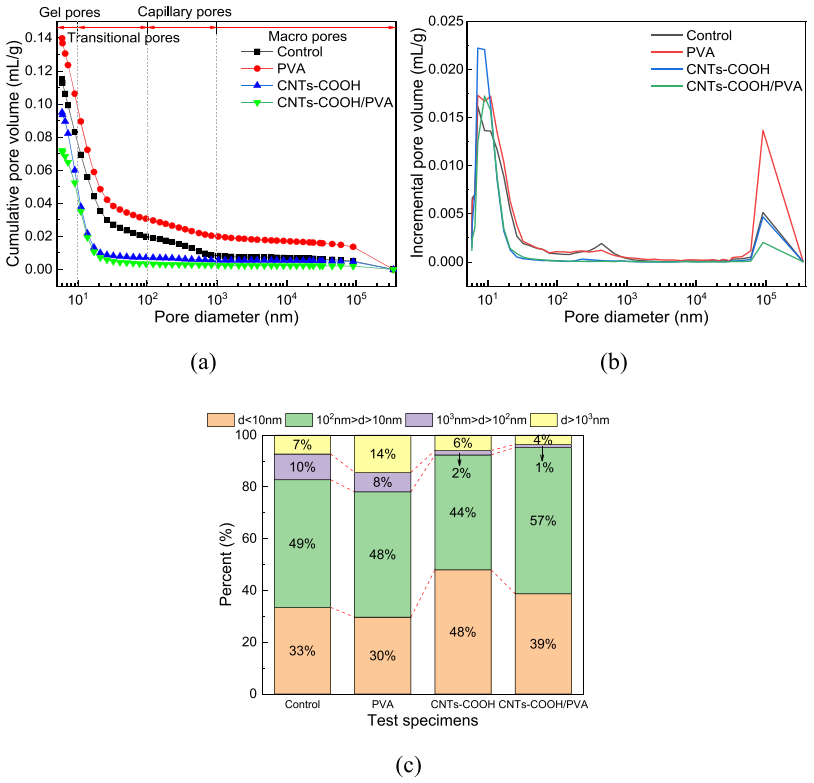

Figure 8. MIP analysis of cement paste with water, PVA solution, CNTs-COOH suspension, and CNTs-COOH/PVA suspension at 28 days, (a) cumulative pore volume distribution, (b) incremental pore volume distribution, and (c) volume proportion of various pores.

addition of PVA can increase the content of $Ca(OH)_2$ at an early age, while CNTs-COOH can promote the formation of C−S−H from $Ca(OH)_2$, thereby improving the 28 days' strength of the cement paste. The above analysis is similar to the results of the XRD experiment. The fact that PVA increases 3 days' hydration degree to 52.47% without increasing strength is analyzed in the pore structure.

3.2.3. Pore Structure Optimization of Cement Paste. For cement-based materials, porosity and pore size distribution are closely related to mechanical properties and are particularly sensitive for flexural strength. Generally, the pores in cement-based materials can be divided into four types: gel pore ($d < 10$ nm), transition pore (10^2 nm $> d > 10$ nm), capillary pore (10^3 nm $> d > 10^2$ nm), and macro pore ($d > 10^3$ nm).[63] The capillary pore and macro pore ($d > 10^2$ nm) have a harmful effect on the mechanical strength of cement-based materials, while the transition pore and gel pore ($d < 10^2$ nm) may influence the shrinkage but have less effect on the mechanical strength.[64,65]

In this section, the CNTs-COOH and PVA concentrations of the suspensions used for cement paste mixing are 0.015 and 0.1%, respectively. The cumulative pore volumes of the control specimen, PVA specimen, CNTs-COOH specimen, and CNTs-COOH/PVA specimen are 0.1152, 0.1398, 0.0950, and 0.0719 mL/g. The results show that the use of PVA alone can introduce more pores into the cement paste, while the addition of CNTs-COOH can fill the pores, as shown in Figure 8a. As shown in Figure 8c, the addition of PVA alone will increase the porosity ratio of the macro pore (14%), which is twice that of the control specimen. This reveals the reason why PVA promotes the hydration process at an early age but cannot improve mechanical strength. On the contrary, the addition of CNTs-COOH alone reduces the capillary pores by 8% compared with the control specimen by transforming them into gel pores, which reflects the filling effects of CNTs-COOH. The enhanced filling effect of CNTs-COOH assisted by PVA not only fills the capillary and macro pores in the cement paste but also convert the pores introduced by PVA into transitional pores. The proportion of the capillary pore and macro pore in the specimen with CNTs-COOH/PVA is only 4 and 1%, respectively, and the proportion of transition pore is as high as 57%. These results are consistent with Figure 8b. It can be concluded from the above analysis that PVA has the function of air intake, mainly introducing large pores affecting mechanical strength, while CNTs-COOH has the filling function to optimize the pore structure. The synergistic effect of the hydration promotion of PVA and the filling of CNTs-COOH achieved the smallest pore volume of the CNTs-COOH/PVA specimen. The flexural strength enhancement effect of the cement paste, which is superior to the compressive strength effect, is attributed to the optimization of the pore structure.

3.2.4. Dispersion Enhancement of CNTs-COOH in Cement Paste. According to the ESEM figure in Figure 9a, a considerable amount of CNTs-COOH without PVA appear in open pores (which precipitate during drying and thus can be seen under a microscope) and present agglomeration, showing relatively poor paste philicity (an analogy to hydrophilicity) and, thus, poor dispersion. However, Figure 9b shows that CNTs-COOH with PVA is well embedded in hydrated cement paste, which could serve as direct evidence of improved paste philicity and indirect evidence of improved dispersion.

To further verify that PVA can promote the nucleation site effect of CNTs-COOH, point scanning of EDS is employed to analyze the content of various elements on the surface of CNTs-COOH. As shown in Figure 9c,e, CNTs-COOH without PVA present a state of multiple entanglements, and the lack of hydrated product attachments on the surface of CNTs-COOH

https://doi.org/10.1021/acsanm.2c00875
ACS Appl. Nano Mater. 2022, 5, 6877−6889

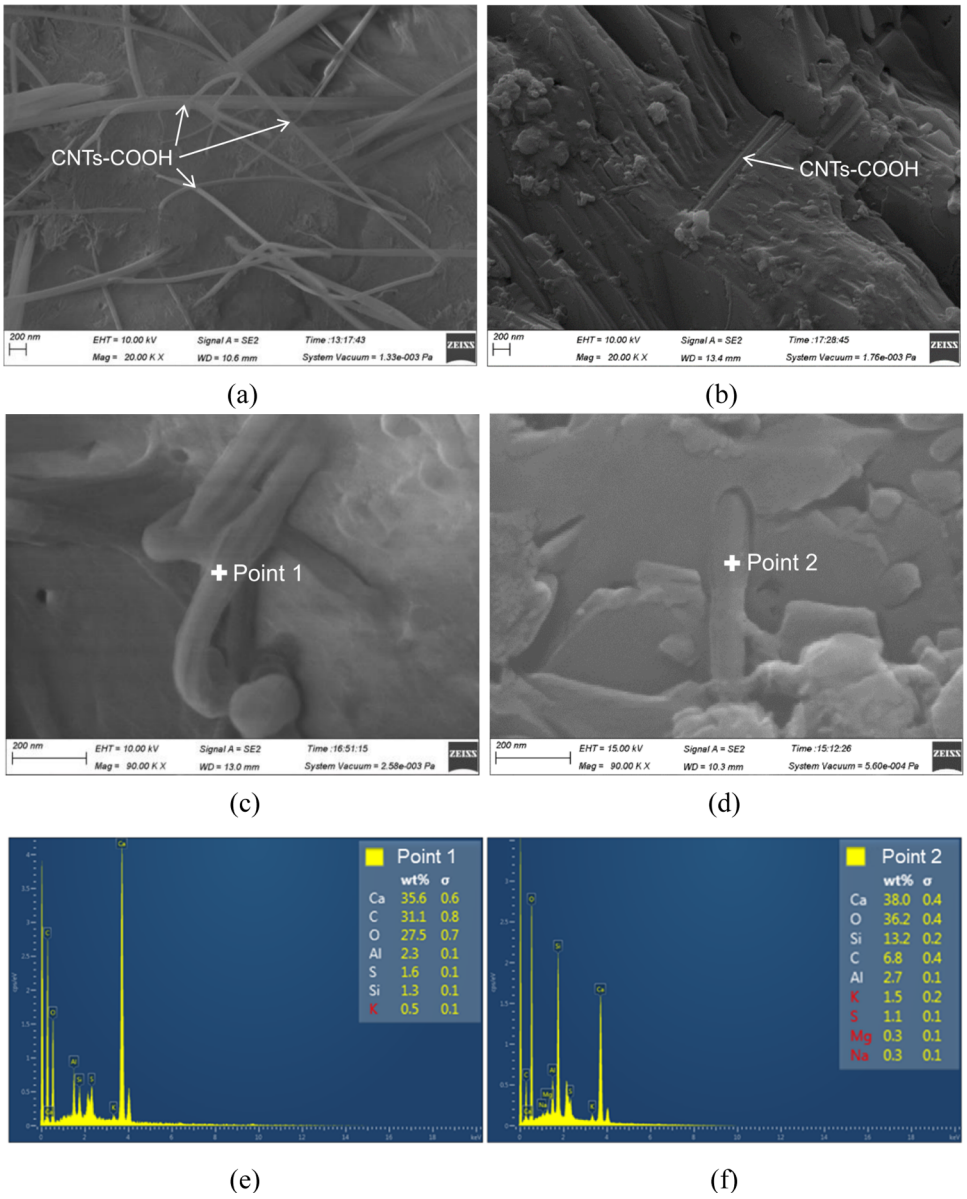

Figure 9. ESEM images and EDS of CNTs-COOH in the cement paste (a, c, e) without PVA, (b, d, f) with PVA.

results in the content of the C element up to 31.1 wt %. The Ca:O:Si:Al of attachments is about 1:2:0:0, which proves that the majority of attachments are $Ca(OH)_2$. On the contrary, the surface of CNTs-COOH modified by PVA contains a large number of hydroxyl groups, which can adsorb abundant hydrated products. The content of the C element is only 6.8 wt % and elements of hydration products are higher on the surface of CNTs-COOH. Ca:O:Si:Al (about 10:23:5:1) indicates that the surface attachments contain calcium silicate hydrate (C−S−H), calcium silicate aluminate hydrate (C−A−S−H), and $Ca(OH)_2$, as shown in Figure 9d,f. These results confirm that PVA can improve the dispersion and nucleation site effect of CNTs-COOH in cement.

3.2.5. Molecular Dynamics Simulation of Interface Enhancement. By pull-out simulation, CNTs-COOH or CNTs-COOH/PVA is pulled out to evaluate the difference in interfacial bonding between them and C−S−H. The pull-out process is shown in Figure 10a,b. The pull-out load−displacement curves of different systems are obtained by counting the applied spring force and displacement (Figure 10c). The curves of Figure 10c show a periodic sawtooth shape, which indicates that the interfacial bonding at the interface between the CNTs-COOH and C−S−H matrix constantly breaks and reorganizes during the pull-out simulation. Comparing the pull-out load before and after PVA addition, it can be found that the maximum pull-out load of CNTs-COOH/PVA/C−S−H is 128 Kcal/mol·Å at 6 and 10 Å and the maximum pull-out load of CNTs-COOH/C−S−H is 78 Kcal/mol·Å at 15 Å, indicating that the introduction of PVA chains increases the maximum pull-out force by 64.1%. After the pull-out displacement exceeds 20 Å, it is obvious that the pull-out force of the two types of interfaces decreases steeply and decays continuously. In the whole pull-out process, the pull-out force of CNTs-COOH/PVA/C−S−H is always higher than that of CNTs-COOH/C−S−H, which fully reveals that the introduction of PVA enhances the interface bonding force.

The difference in the atoms' local structure at the interface before and after the addition of PVA is analyzed to explain that

https://doi.org/10.1021/acsanm.2c00875
ACS Appl. Nano Mater. 2022, 5, 6877−6889

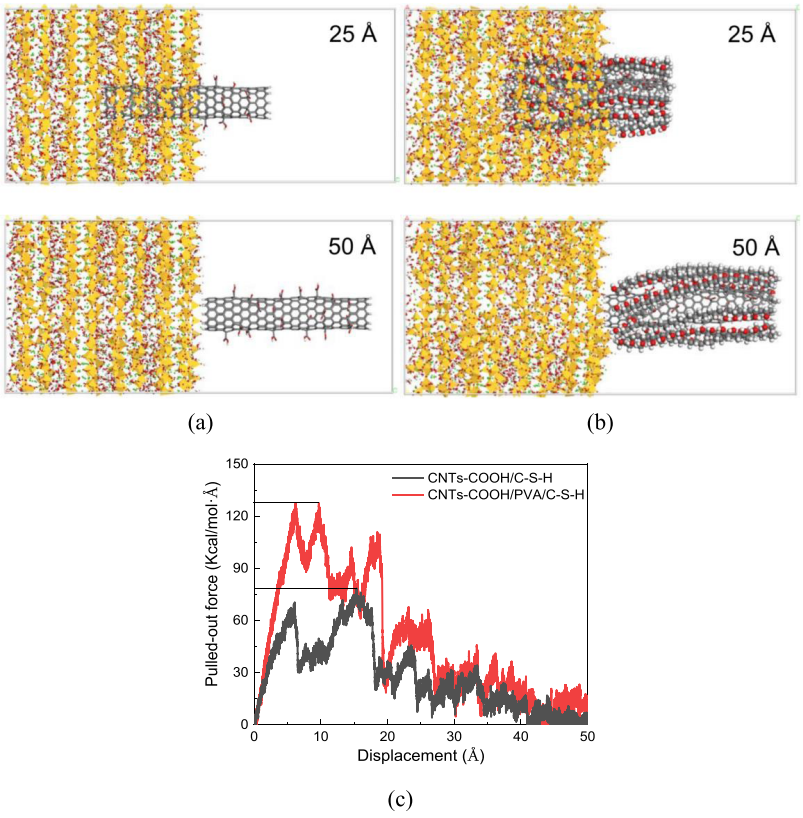

Figure 10. Pull-out process of (a) CNTs-COOH/C−S−H model and (b) CNTs-COOH/PVA/C−S−H model. (c) Pull-out load−displacement curves of models.

the interaction between CNTs-COOH/PVA and C−S−H is much stronger than that between CNTs-COOH and C−S−H. The radial distribution function (RDF) as an effective means of evaluating spatial correlations between atoms is employed to characterize bonding between atoms at interfaces. The RDF curves in different systems are calculated as shown in Figure 11. For the CNTs-COOH/C−S−H model, there are significant peaks of the RDFs between interlayer Ca and oxygen on silicon chains (O_b) and polar oxygen on top of CNTs-COOH (O_{CNT}), as shown in Figure 11a. This indicates that Ca at the interface is able to bridge the CNTs-COOH and the C−S−H with the oxygen atoms above them to form an O_b-Ca-O_{CNT} connection. The ion-pair network is illustrated in Figure 11b, which is the source of the interfacial interactions between CNTs-COOH and C−S−H.

When PVA is introduced, the ion-pair connection mechanism at the interface is changed. As shown in Figure 11c, the RDF curves between $Ca-O_b$ and $Ca-O_w$ are almost unaffected after PVA addition. The peak of $Ca-O_{CNT}$ RDF is slightly reduced. Most importantly, there is a significant peak between oxygen above PVA (O_{PVA}) and Ca at the interface, indicating that the introduction of PVA forms a new ion pair (O_b-Ca-O_{PVA}) (Figure 11d). The RDF analysis reveals that the introduction of PVA changes the ion-pair species at the interface, and the additional O_b-Ca-O_{PVA} form could further enhance the interfacial interactions at the interface, which directly explains the significant increase in the pull-out force. In addition, there are also clear peaks in the RDF curves between the hydroxyl group on the PVA and the hydroxyl group on the surface of the C−S−H substrate (Figure 11e). This indicates that the introduction of PVA can not only form new ion pairs but also develop new hydrogen-bonding connections ($O_{PVA}-H_{CSH}$ and $H_{PVA}-O_{CSH}$) at the interface (Figure 11f), thus further enhancing the interaction on the interface.

4. CONCLUSIONS

In this paper, a synergistic effect of CNTs-COOH and PVA on the enhancement of cement paste has been systematically investigated, with a view to meeting concrete performance with less cement in the future. According to the results of experiments and analysis, the following conclusions can be drawn:

(1) The adsorption of PVA on the surface of CNTs-COOH enhances the dispersion effect of suspensions with different CNTs-COOH contents by more than 44%, and CNTs-COOH/PVA suspensions maintain better dispersion stability.

(2) After mixing with CNTs-COOH/PVA suspensions, the enhancement of the flexural strength of cement paste is much higher than that of compressive strength, and the enhancement of 3 days is much higher than that of 7 days and 28 days.The 0.015% CNTs-COOH/0.1% PVA suspension enhances the flexural strength of cement paste specimens by 73, 32, and 42% at 3, 7, and 28 days.

(3) For the cement matrix, CNTs-COOH can promote the early degree of hydration and gradually convert $Ca(OH)_2$ promoted by PVA to C−S−H, which contributes to 3 days and 28 days' mechanical strength of cement paste. Meanwhile, CNTs-COOH has the function of filling to optimize large-diameter pores introduced by PVA, thus further enhancing the flexural strength of the cement paste.

(4) For the interface, PVA could disperse CNTs-COOH individually in the cement paste and enhance its

https://doi.org/10.1021/acsanm.2c00875
ACS Appl. Nano Mater. 2022, 5, 6877−6889

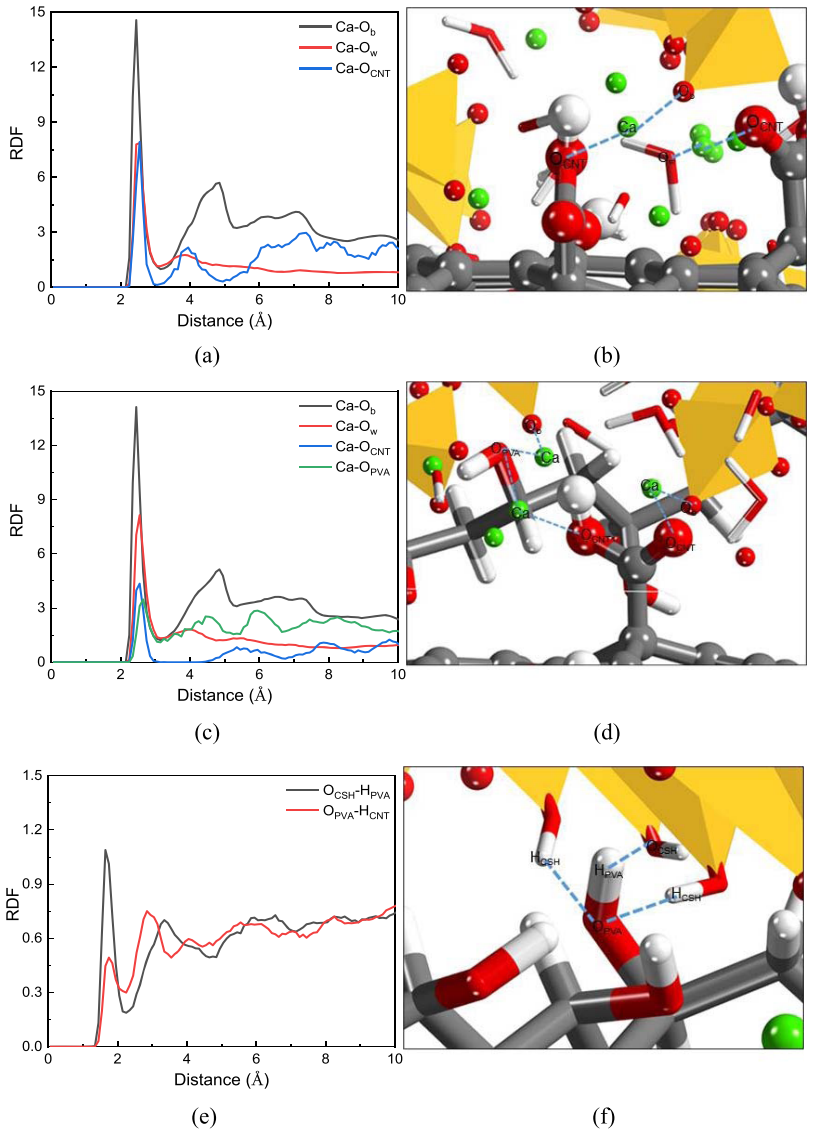

Figure 11. RDFs of the (a) CNTs-COOH/C−S−H model and (c, e) CNTs-COOH/PVA/C−S−H model. The snapshots of the ion-pair networks of (b) CNTs-COOH/C−S−H model and (d, f) CNTs-COOH/PVA/C−S−H model.

nucleation site effect by increasing the content of C−S−H at the interface. The pull-out simulation results indicate that the peak of pull-out force increases by 64.1% after the introduction of PVA, indicating that the interfacial bonding between C−S−H and CNTs-COOH/PVA is stronger than that between C−S−H and CNTs-COOH. RDF analysis reveals that the enhancement of the interface is attributed to the fact that PVA can form ion pairs (O_b−Ca−O_{PVA}) and hydrogen bonds (O_{PVA}−H_{CSH} and H_{PVA}−O_{CSH}).

■ ASSOCIATED CONTENT

Supporting Information

The Supporting Information is available free of charge at https://pubs.acs.org/doi/10.1021/acsanm.2c00875.

Chemical compositions of cement, characteristics of carboxylated carbon nanotubes, morphology of carboxylated carbon nanotubes, mix proportions of suspensions, and cost analysis (PDF)

■ AUTHOR INFORMATION

Corresponding Author

Jinrui Zhang − *State Key Laboratory of Hydraulic Engineering Simulation and Safety, Tianjin University, Tianjin 300072, China;* orcid.org/0000-0003-2269-7315; Email: jinrui.zhang@tju.edu.cn

Authors

Yuyang Zhao − *State Key Laboratory of Hydraulic Engineering Simulation and Safety, Tianjin University, Tianjin 300072, China;* orcid.org/0000-0002-2426-1091

Gang Qiao − *Department of Civil Engineering, Qingdao University of Technology, Qingdao 266000, China*

Dongshuai Hou − *Department of Civil Engineering, Qingdao University of Technology, Qingdao 266000, China;* orcid.org/0000-0002-1252-2987

Biqin Dong − *Guangdong Province Key Laboratory of Durability for Marine Civil Engineering, Shenzhen University, Shenzhen 518060, China*

Hongyan Ma − *Department of Civil, Architectural and Environmental Engineering, Missouri University of Science and*

https://doi.org/10.1021/acsanm.2c00875
ACS Appl. Nano Mater. 2022, 5, 6877−6889

Technology, Rolla, Missouri 65401, United States;
orcid.org/0000-0003-3674-3845

Complete contact information is available at:
https://pubs.acs.org/10.1021/acsanm.2c00875

Notes

The authors declare no competing financial interest.

■ ACKNOWLEDGMENTS

This work was financially supported by the National Natural Science Foundation of China under the grants 52078332, U2006223, and 51925805, the Natural Science Foundation of Hebei Province under the grant E2020402079, and the Guangdong Provincial Key Laboratory of Durability for Marine Civil Engineering (SZU) under the grant 2020B1212060074.

■ REFERENCES

(1) Němeček, J.; Králík, V.; Šmilauer, V.; Polívka, L.; Jäger, A. Tensile strength of hydrated cement paste phases assessed by micro-bending tests and nanoindentation. *Cem. Concr. Compos.* **2016**, *73*, 164−173.
(2) Yoo, D.-Y.; Oh, T.; Kang, M.-C.; Kim, M.-J.; Choi, H.-J. Enhanced tensile ductility and sustainability of high-strength strain-hardening cementitious composites using waste cement kiln dust and oxidized polyethylene fibers. *Cem. Concr. Compos.* **2021**, *120*, No. 104030.
(3) Dauber-Osguthorpe, P.; Roberts, V. A.; Osguthorpe, D. J.; Wolff, J.; Genest, M.; Hagler, A. T. Structure and energetics of ligand binding to proteins: Escherichia coli dihydrofolate reductase-trimethoprim, a drug-receptor system. *Proteins: Struct., Funct., Bioinf.* **1988**, *4*, 31−47.
(4) Park, H. G.; Hwang, H. J.; Hong, G. H.; Kim, Y. N.; Kim, J. Y. Slab Construction Load Affected by Shore Stiffness and Concrete Cracking. *ACI Struct. J.* **2011**, *108*, 679−688.
(5) Shi, N.; Ouyang, J.; Zhang, R.; Huang, D. Experimental Study on Early-Age Crack of Mass Concrete under the Controlled Temperature History. *Adv. Mater. Sci. Eng.* **2014**, *2014*, 1−10.
(6) Xin, J. D.; Zhang, G. X.; Liu, Y.; Wang, Z. H.; Wu, Z. Effect of temperature history and restraint degree on cracking behavior of early-age concrete. *Constr. Build. Mater.* **2018**, *192*, 381−390.
(7) Ma, H.; Li, Z. Microstructures and mechanical properties of polymer modified mortars under distinct mechanisms. *Constr. Build. Mater.* **2013**, *47*, 579−587.
(8) Ramezani, M.; Kim, Y. H.; Sun, Z. Modeling the mechanical properties of cementitious materials containing CNTs. *Cem. Concr. Compos.* **2019**, *104*, No. 103347.
(9) Yan, L. Y.; Chen, H.; Li, P.; Kim, D. H.; Chan-Park, M. B. Finely dispersed single-walled carbon nanotubes for polysaccharide hydrogels. *ACS Appl. Mater. Interfaces* **2012**, *4*, 4610−4615.
(10) Avasthi, P.; Kumar, A.; Balakrishnan, V. Aligned CNT Forests on Stainless Steel Mesh for Flexible Supercapacitor Electrode with High Capacitance and Power Density. *ACS Appl. Nano Mater.* **2019**, *2*, 1484−1495.
(11) Kobashi, K.; Sekiguchi, A.; Yamada, T.; Muroga, S.; Okazaki, T. Dispersions of High-Quality Carbon Nanotubes with Narrow Aggregate Size Distributions by Viscous Liquid for Conducting Polymer Composites. *ACS Appl. Nano Mater.* **2020**, *3*, 1391−1399.
(12) Kirmani, M. H.; Sachdeva, G.; Pandey, R.; Odegard, G. M.; Liang, R.; Kumar, S. Cure Behavior Changes and Compression of Carbon Nanotubes in Aerospace Grade Bismaleimide-Carbon Nanotube Sheet Nanocomposites. *ACS Appl. Nano Mater.* **2021**, *4*, 2476−2485.
(13) Pan, H.; She, W.; Zuo, W.; Zhou, Y.; Huang, J.; Zhang, Z.; Geng, Z.; Yao, Y.; Zhang, W.; Zheng, L.; Miao, C.; Liu, J. Hierarchical Toughening of a Biomimetic Bulk Cement Composite. *ACS Appl. Mater. Interfaces* **2020**, *12*, 53297−53309.
(14) Du, M. R.; Chen, S. J.; Duan, W. H.; Chen, W. Q.; Jing, H. W. Role of Multiwalled Carbon Nanotubes as Shear Reinforcing Nanopins in Quasi-Brittle Matrices. *ACS Appl. Nano Mater.* **2018**, *1*, 1731−1740.
(15) Sobolkina, A.; Mechtcherine, V.; Khavrus, V.; Maier, D.; Mende, M.; Ritschel, M.; Leonhardt, A. Dispersion of carbon nanotubes and its influence on the mechanical properties of the cement matrix. *Cem. Concr. Compos.* **2012**, *34*, 1104−1113.
(16) Lu, Z.; Hou, D.; Meng, L.; Sun, G.; Lu, C.; Li, Z. Mechanism of cement paste reinforced by graphene oxide/carbon nanotubes composites with enhanced mechanical properties. *RSC Adv.* **2015**, *5*, 100598−100605.
(17) Isfahani, F. T.; Li, W.; Redaelli, E. Dispersion of multi-walled carbon nanotubes and its effects on the properties of cement composites. *Cem. Concr. Compos.* **2016**, *74*, 154−163.
(18) Ma, P.-C.; Mo, S.-Y.; Tang, B.-Z.; Kim, J.-K. Dispersion, interfacial interaction and re-agglomeration of functionalized carbon nanotubes in epoxy composites. *Carbon* **2010**, *48*, 1824−1834.
(19) Zhang, J.; Ke, Y.; Zhang, J.; Han, Q.; Dong, B. Cement paste with well-dispersed multi-walled carbon nanotubes: Mechanism and performance. *Constr. Build. Mater.* **2020**, *262*, No. 120746.
(20) Li, G. Y.; Wang, P. M.; Zhao, X. Mechanical behavior and microstructure of cement composites incorporating surface-treated multi-walled carbon nanotubes. *Carbon* **2005**, *43*, 1239−1245.
(21) Mansouri Sarvandani, M.; Mahdikhani, M.; Aghabarati, H.; Haghparast Fatmehsari, M. Effect of functionalized multi-walled carbon nanotubes on mechanical properties and durability of cement mortars. *J. Build. Eng.* **2021**, *41*, No. 102407.
(22) Savilov, S. V.; Ivanov, A. S.; Egorov, A. V.; Kirikova, M. N.; Arkhipova, E. A.; Lunin, V. V. Effect of the morphology of structured carbon nanomaterials on their oxidizability. *Russ. J. Phys. Chem. A* **2016**, *90*, 429−435.
(23) Xia, T.; Guo, X.; Lin, Y.; Xin, B.; Li, S.; Yan, N.; Zhu, L. Aggregation of oxidized multi-walled carbon nanotubes: Interplay of nanomaterial surface O-functional groups and solution chemistry factors. *Environ. Pollut.* **2019**, *251*, 921−929.
(24) Sung, J. H.; Hwang, M.-R.; Kim, J. O.; Lee, J. H.; Kim, Y. I.; Kim, J. H.; Chang, S. W.; Jin, S. G.; Kim, J. A.; Lyoo, W. S.; Han, S. S.; Ku, S. K.; Yong, C. S.; Choi, H.-G. Gel characterisation and in vivo evaluation of minocycline-loaded wound dressing with enhanced wound healing using polyvinyl alcohol and chitosan. *Int. J. Pharm.* **2010**, *392*, 232−240.
(25) Xiong, X. B.; Liu, C.; Ni, X. Y.; Liang, C. Q.; Zeng, X. R. Polyvinyl Alcohol/Graphene Oxide Interlayer for Enhancing Adhesive Performance of HA Coating on C/C Composites Prepared by Hydrothermal Electrodeposition/Hydrothermal Treatment. *ACS Appl. Mater. Interfaces* **2020**, *12*, 55710−55722.
(26) Thong, C. C.; Teo, D. C. L.; Ng, C. K. Application of polyvinyl alcohol (PVA) in cement-based composite materials: A review of its engineering properties and microstructure behavior. *Constr. Build. Mater.* **2016**, *107*, 172−180.
(27) Wang, W.; Li, Z.; Prestat, E.; Hashimoto, T.; Guan, J.; Kim, K. S.; Kingston, C. T.; Simard, B.; Young, R. J. Reinforcement of Polymer-Based Nanocomposites by Thermally Conductive and Electrically Insulating Boron Nitride Nanotubes. *ACS Appl. Nano Mater.* **2020**, *3*, 364−374.
(28) Fan, J.; Li, G.; Deng, S.; Wang, Z. Mechanical Properties and Microstructure of Polyvinyl Alcohol (PVA) Modified Cement Mortar. *Appl. Sci.* **2019**, *9*, No. 2178.
(29) Pique, T. M.; Vazquez, A. Control of hydration rate of polymer modified cements by the addition of organically modified montmorillonites. *Cem. Concr. Compos.* **2013**, *37*, 54−60.
(30) Lu, Z.; Hanif, A.; Lu, C.; Sun, G.; Cheng, Y.; Li, Z. Thermal, mechanical, and surface properties of poly(vinyl alcohol) (PVA) polymer modified cementitious composites for sustainable development. *J. Appl. Polym. Sci.* **2018**, *135*, No. 46177.
(31) Xie, Y.; Lin, X.; Li, H.; Ji, T. Effect of polyvinyl alcohol powder on the bonding mechanism of a new magnesium phosphate cement mortar. *Constr. Build. Mater.* **2020**, *239*, No. 117871.
(32) Wu, M. L.; Chen, Y.; Zhang, L.; Zhan, H.; Qiang, L.; Wang, J. N. High-Performance Carbon Nanotube/Polymer Composite Fiber from Layer-by-Layer Deposition. *ACS Appl. Mater. Interfaces* **2016**, *8*, 8137−8144.

(33) Zhang, M.; Yeow, J. T. W. Flexible Polymer-Carbon Nanotube Composite with High-Response Stability for Wearable Thermal Imaging. *ACS Appl. Mater. Interfaces* **2018**, *10*, 26604−26609.
(34) Güler, Ö.; Cacim, N. N.; Evin, E.; Yahia, I. S. The synergistic effect of CNTs-polymeric surfactant on the properties of concrete nanocomposites: Comparative study. *J. Compos. Mater.* **2021**, *55*, 1371−1384.
(35) Park, O.-K.; Lee, J. H. Carbon nanotube-poly(vinyl alcohol) hybrid aerogels: Improvements in the surface area and structural stability by internal morphology control. *Composites, Part B* **2018**, *144*, 229−236.
(36) Sridharan, S.; Choi, K.-H. Fabrication of flexible SWCNT thin films through electrohydrodynamic atomization technique and investigation of their electrical properties. *Mater. Lett.* **2014**, *115*, 215−218.
(37) Han, Q.; Yang, Y.; Zhang, J.; Yu, J.; Hou, D.; Dong, B.; Ma, H. Insights into the interfacial strengthening mechanism of waste rubber/cement paste using polyvinyl alcohol: Experimental and molecular dynamics study. *Cem. Concr. Compos.* **2020**, *114*, No. 103791.
(38) Alafogianni, P.; Dassios, K.; Tsakiroglou, C. D.; Matikas, T. E.; Barkoula, N. M. Effect of CNT addition and dispersive agents on the transport properties and microstructure of cement mortars. *Constr. Build. Mater.* **2019**, *197*, 251−261.
(39) Wang, Z.; Yu, J.; Li, G.; Zhang, M.; Leung, C. K. Y. Corrosion behavior of steel rebar embedded in hybrid CNTs-OH/polyvinyl alcohol modified concrete under accelerated chloride attack. *Cem. Concr. Compos.* **2019**, *100*, 120−129.
(40) Lavagna, L.; Nisticò, R.; Musso, S.; Pavese, M. Functionalization as a way to enhance dispersion of carbon nanotubes in matrices: a review. *Mater. Today Chem.* **2021**, *20*, No. 100477.
(41) Ma, H. Mercury intrusion porosimetry in concrete technology: tips in measurement, pore structure parameter acquisition and application. *J. Porous Mater.* **2014**, *21*, 207−215.
(42) Ma, H. Y.; Li, Z. J. Realistic pore structure of Portland cement paste: experimental study and numerical simulation. *Comput. Concr.* **2013**, *11*, 317−336.
(43) Lu, Z.; Chen, B.; Leung, C. Y.; Li, Z.; Sun, G. Aggregation size effect of graphene oxide on its reinforcing efficiency to cement-based materials. *Cem. Concr. Compos.* **2019**, *100*, 85−91.
(44) Qiao, G.; Hou, D.; Wang, P.; Lu, Z. Insights on failure modes of calcium-silicate-hydrate interface strengthened by polyacrylamides: Structure, dynamic and mechanical properties. *Constr. Build. Mater.* **2021**, *278*, No. 122406.
(45) Shahsavari, R.; Pellenq, R. J.; Ulm, F. J. Empirical force fields for complex hydrated calcio-silicate layered materials. *Phys. Chem. Chem. Phys.* **2011**, *13*, 1002−1011.
(46) Hou, D.; Zhao, T.; Wang, P.; Li, Z.; Zhang, J. Molecular dynamics study on the mode I fracture of calcium silicate hydrate under tensile loading. *Eng. Fract. Mech.* **2014**, *131*, 557−569.
(47) Kai, M. F.; Zhang, L. W.; Liew, K. M. New insights into creep characteristics of calcium silicate hydrates at molecular level. *Cem. Concr. Res.* **2021**, *142*, No. 106366.
(48) Zhou, Y.; Hou, D.; Manzano, H.; Orozco, C. A.; Geng, G.; Monteiro, P. J. M.; Liu, J. Interfacial Connection Mechanisms in Calcium-Silicate-Hydrates/Polymer Nanocomposites: A Molecular Dynamics Study. *ACS Appl. Mater. Interfaces* **2017**, *9*, 41014−41025.
(49) Hou, D.; Yu, J.; Wang, P. Molecular dynamics modeling of the structure, dynamics, energetics and mechanical properties of cement-polymer nanocomposite. *Composites, Part B* **2019**, *162*, 433−444.
(50) Sakhavand, N.; Muthuramalingam, P.; Shahsavari, R. Toughness governs the rupture of the interfacial H-bond assemblies at a critical length scale in hybrid materials. *Langmuir* **2013**, *29*, 8154−8163.
(51) Zhou, Y.; Tang, L.; Liu, J.; Miao, C. Interaction mechanisms between organic and inorganic phases in calcium silicate hydrates/poly(vinyl alcohol) composites. *Cem. Concr. Res.* **2019**, *125*, No. 105891.
(52) Chou, C.-S.; Huang, C.-I.; Yang, R.-Y.; Wang, C.-P. The effect of SWCNT with the functional group deposited on the counter electrode on the dye-sensitized solar cell. *Adv. Powder Technol.* **2010**, *21*, 542−550.
(53) Mansur, H. S.; Sadahira, C. M.; Souza, A. N.; Mansur, A. A. P. FTIR spectroscopy characterization of poly (vinyl alcohol) hydrogel with different hydrolysis degree and chemically crosslinked with glutaraldehyde. *Mater. Sci. Eng.: C* **2008**, *28*, 539−548.
(54) Zhang, H.; Zhang, J. The preparation of novel polyvinyl alcohol (PVA)-based nanoparticle/carbon nanotubes (PNP/CNTs) aerogel for solvents adsorption application. *J. Colloid Interface Sci.* **2020**, *569*, 254−266.
(55) Cui, X.; Han, B.; Zheng, Q.; Yu, X.; Dong, S.; Zhang, L.; Ou, J. Mechanical properties and reinforcing mechanisms of cementitious composites with different types of multiwalled carbon nanotubes. *Composites, Part A* **2017**, *103*, 131−147.
(56) Deboucha, W.; Leklou, N.; Khelidj, A.; Oudjit, M. N. Hydration development of mineral additives blended cement using thermogravimetric analysis (TGA): Methodology of calculating the degree of hydration. *Constr. Build. Mater.* **2017**, *146*, 687−701.
(57) Monteagudo, S. M.; Moragues, A.; Gálvez, J. C.; Casati, M. J.; Reyes, E. The degree of hydration assessment of blended cement pastes by differential thermal and thermogravimetric analysis. Morphological evolution of the solid phases. *Thermochim. Acta* **2014**, *592*, 37−51.
(58) Pane, I.; Hansen, W. Investigation of blended cement hydration by isothermal calorimetry and thermal analysis. *Cem. Concr. Res.* **2005**, *35*, 1155−1164.
(59) Mounanga, P.; Khelidj, A.; Loukili, A.; Baroghel-Bouny, V. Predicting Ca(OH)2 content and chemical shrinkage of hydrating cement pastes using analytical approach. *Cem. Concr. Res.* **2004**, *34*, 255−265.
(60) Loukili, A.; Khelidj, A.; Richard, P. Hydration kinetics, change of relative humidity, and autogenous shrinkage of ultra-high-strength concrete. *Cem. Concr. Res.* **1999**, *29*, 577−584.
(61) Bai, R.; Zhang, J.; Yan, C.; Liu, S.; Wang, X.; Yang, Z. Calcium hydroxide content and hydration degree of cement in cementitious composites containing calcium silicate slag. *Chemosphere* **2021**, *280*, No. 130918.
(62) Han, B.; Zhang, L.; Zeng, S.; Dong, S.; Yu, X.; Yang, R.; Ou, J. Nano-core effect in nano-engineered cementitious composites. *Composites, Part A* **2017**, *95*, 100−109.
(63) Ahmad, M. R.; Chen, B.; Yu, J. A comprehensive study of basalt fiber reinforced magnesium phosphate cement incorporating ultrafine fly ash. *Composites, Part B* **2019**, *168*, 204−217.
(64) Li, Y.; Li, J. Capillary tension theory for prediction of early autogenous shrinkage of self-consolidating concrete. *Constr. Build. Mater.* **2014**, *53*, 511−516.
(65) Pu, S.; Zhu, Z.; Song, W.; Huo, W.; Zhang, J. Mechanical and microscopic properties of fly ash phosphoric acid-based geopolymer paste: A comprehensive study. *Constr. Build. Mater.* **2021**, *299*, No. 123947.

https://doi.org/10.1021/acsanm.2c00875
ACS Appl. Nano Mater. 2022, 5, 6877−6889